European Conference on Computational Fluid Dynamics
ECCOMAS CFD 2006
P. Wesseling, E. Oñate, J. Périaux (Eds)

EFFECTS OF FLUID-STRUCTURE INTERACTION ON THE TRAILING-EDGE NOISE

Youngmin Bae*, Jae Young Jang[+] and Young J. Moon[+]

*†Korea University
Department of Mechanical Engineering,
1 Anam-dong, Sungbuk-ku, Seoul, Korea
e-mail: *oioooo@korea.ac.kr, [+]scaner007@korea.ac.kr, [+]yjmoon@korea.ac.kr
Web page: http://cfd.korea.ac.kr

Key words: Trailing-Edge Noise, Fluid-Structure Interaction (FSI), Noise Reduction, Wake Instability, Karman vortex

Abstract. *In the present study, the effects of fluid-structure interaction (FSI) on the trailing-edge noise are numerically investigated, particularly for the cases of wake instability and Karman vortex shedding. The trailing-edge is modelled as a flat plate with an elastic cantilever end and its flow-induced vibration is solved by an eigenmode analysis with the Galerkin method. The FSI analysis is conducted in a fully coupled manner with direct numerical simulation (DNS) of the flow and sound. Computed solutions for the wake instability show that when the first-eigenmode natural frequency (ω_n) of the cantilever is close to be resonant with the wake characteristic frequency (ω_c), the sound pressure level (SPL) is significantly reduced by -20 dB or increased by +15 dB, depending on the ratio of ω_n/ω_c. For Karman vortex shedding, the flow and acoustic details are somewhat different but FSI also has considerable impacts on the SPL and directivity, if ω_n is close to ω_c.*

1 INTRODUCTION

Trailing-edge noise is an important noise source for airfoils or fan blades. It could be generated by wake instability, Karman vortex shedding, or edge-scattering of the turbulent boundary layer eddies[1]. Comprehensive experimental investigation[2], analytical modeling works[3,4], and computations[5,6] on the trailing-edge noise have been conducted for years. There also have been some efforts to reduce the trailing-edge noise by modifying the blunt trailing-edge profile[8] or implementing a porous media to the trailing-edge[9]. Recently, Herr and Dobrzynski[10] adopted a brush to the trailing-edge to reduce the trailing-edge noise.

In the present study, a fluid-structure interaction (FSI) effect is considered to reduce the trailing-edge noise. As shown in Fig. 1, the trailing-edge is modeled as a flat plate with an elastic cantilever end and its flow-induced vibration is solved by an eigenmode analysis with the Galerkin method. The beam equation is solved in a fully coupled manner with direct numerical simulation (DNS) of the flow and sound. The DNS solution is obtained by solving the two-dimensional compressible Navier-Stokes equations in a moving coordinate system

with a sixth-order compact finite difference scheme and four-stage Runge-Kutta method for space and time, respectively.

First, the trailing-edge noise generated by wake instability is considered at Re_h=200 and M=0.4. For the rigid trailing-edge, a dipole tone is generated at $St_w=fh/U$=0.05, which corresponds to the most unstable mode[1] in the wake instability. The natural frequency of the elastic cantilever is a function of its eigenvalues, speed of sound and fluid density, aspect ratio (h/L, L: cantilever length), and elasticity of the cantilever. Second, the trailing-edge noise generated by Karman vortex shedding is considered at Re_h=1000 and M=0.4. For the rigid trailing-edge, a much stronger dipole tone is produced at St_k=0.177. In this study, the FSI effects on the acoustic characteristics of the trailing-edge are scrutinized with various elastic properties of the cantilever beam.

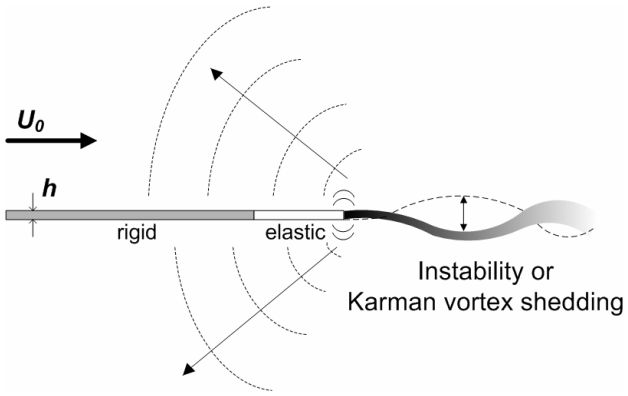

Figure 1 : Schematic of trailing-edge noise generation with FSI effect included

2 METHODOLOGIES

In the present study, the effects of fluid-structure interaction (FSI) on the trailing-edge noise are numerically investigated with a simplified computational model. The flow and acoustic fields are computed by direct numerical simulation (DNS) of the full compressible Navier-Stokes equations. The beam equation is solved in a fully coupled manner with the DNS. Computational methods are described below, including moving grid system and eigenmode analysis of the elastic cantilever beam.

2.1 Direct numerical simulation (DNS)

The DNS solution is obtained by solving the two-dimensional, compressible Navier-Stokes equations, written as

$$\frac{\partial Q}{\partial t}+\frac{\partial E}{\partial x}+\frac{\partial F}{\partial y}=\frac{\partial E_v}{\partial x}+\frac{\partial F_v}{\partial y}, \tag{1}$$

and

$$Q=\begin{bmatrix}\rho\\ \rho u\\ \rho v\\ \rho e\end{bmatrix},\quad E=\begin{bmatrix}\rho u\\ \rho u^2+p\\ \rho uv\\ u(e+p)\end{bmatrix},\quad F=\begin{bmatrix}\rho v\\ \rho uv\\ \rho v^2+p\\ v(e+p)\end{bmatrix}$$

$$E_v=\begin{bmatrix}0\\ \tau_{xx}\\ \tau_{xy}\\ u\tau_{xx}+v\tau_{xy}-q_x\end{bmatrix},\quad F_v=\begin{bmatrix}0\\ \tau_{xy}\\ \tau_{yy}\\ u\tau_{xy}+v\tau_{yy}-q_y\end{bmatrix}. \tag{2}$$

where τ_{xx},τ_{xy} and τ_{yy} indicate viscous dissipation terms and q_x,q_y are neglected.

In order to include the effects of wall deformation of the elastic trailing-edge, the governing equations are solved in a moving coordinate system. The components of the transformation matrix between the physical space (x, y, t) and the computational space (ξ, η, τ) are defined as

$$\begin{bmatrix}d\tau\\ d\xi\\ d\eta\end{bmatrix}=\begin{bmatrix}1 & 0 & 0\\ \xi_t & \xi_x & \xi_y\\ \eta_t & \eta_x & \eta_y\end{bmatrix}\begin{bmatrix}dt\\ dx\\ dy\end{bmatrix}, \tag{3}$$

where

$$\begin{aligned}&\xi_x=\frac{y_\eta}{J},\quad \xi_y=-\frac{x_\eta}{J},\quad \eta_x=-\frac{y_\xi}{J},\quad \eta_y=\frac{x_\xi}{J}\\ &\xi_t=\frac{(-x_\tau y_\eta+x_\eta y_\tau)}{J},\quad \eta_t=\frac{(x_\tau y_\xi-x_\xi y_\tau)}{J},\quad \tau=t\end{aligned}. \tag{4}$$

Here, $J=x_\xi y_\eta-x_\eta y_\xi$, and x_τ and y_τ represent moving velocities at each control surface.

The governing equations are integrated in time by a four-stage Runge-Kutta method and spatially discretized with a sixth-order compact finite difference scheme[11]. The first and second derivatives with respect to x are implicitly calculated with a five stencil, i.e.

$$\begin{aligned}&\alpha_1 f'_{i-1}+f'_i+\alpha_1 f'_{i+1}=a_1\frac{f_{i+1}-f_{i-1}}{2\Delta x}+b_1\frac{f_{i+2}-f_{i-2}}{4\Delta x}\\ &\alpha_2 f''_{i-1}+f''_i+\alpha_2 f''_{i+1}=a_2\frac{f_{i+1}-2f_i+f_{i-1}}{\Delta x^2}+b_2\frac{f_{i+2}-2f_i+f_{i-2}}{4\Delta x^2}\end{aligned} \tag{5}$$

where α_1=1/3, α_2=2/11, a_1=14/9, b_1=1/9, a_2=12/11, and b_2=3/11.

Practically, when using a high order scheme to the stretched meshes, numerical instability are encountered due to numerical truncations or failure of capturing high wave-number phenomena. Thus, a tenth-order spatial filtering proposed by Gaitonde et al.[12] is applied every iteration to suppress the high frequency errors that might be caused by grid non-uniformity. For the far-field boundary condition, an energy transfer and annihilation (ETA) boundary condition[13] with buffer zone is used for not allowing any reflection of out-going waves.

2.2 Fluid-structure interaction (FSI)

In this study, the trailing-edge is modeled as a flat plat with an elastic cantilever end and so its vertical displacement is written as[14]

$$\frac{\partial^2}{\partial x^2}\left[EI(x)\frac{\partial^2 y(x,t)}{\partial x^2} \right] + m(x)\frac{\partial^2 y(x,t)}{\partial t^2} = f(x,t), \qquad 0 < x < L \tag{6}$$

where $EI(x)$ is a flexural rigidity, $m(x)$ is the mass per unit length, $f(x,t)$ represents the force distributed over the elastic region, and L is the length of the trailing-edge. The force on the elastic cantilever beam is usually involved with pressure and shear stress but it is assumed that shear stress is negligible compared to pressure. In this study, the flow-induced vibration is solved by an eigenmode analysis with the Galerkin method,

$$y(x,t) = \sum_{r=1}^{\infty} Y_r(x)\eta_r(t), \tag{7}$$

where r is the mode number, $Y_r(x)$ and $\eta_r(t)$ represent the modal shape and modal coordinates, respectively. By substituting Eq. (7) into Eq. (6) and applying an orthogonality of the natural modes, an ordinary differential equation of the modal coordinates can be derived

$$\ddot{\eta}_r(t) + \omega_r^2 \eta_r(t) = \int_0^L Y_r(x) f(x,t) dx, \qquad r = 1, 2, \cdots. \tag{8}$$

An analytic solution for the modal shape, $Y_r(x)$[15] can be obtained by employing a fixed left-end boundary condition for the cantilever beam, and is written by

$$Y_r(x) = \cosh \beta_r x - \cos \beta_r x - \sigma_r (\sinh \beta_r x - \sin \beta_r x), \tag{9}$$

where

$$\sigma_r = \frac{\sinh \beta_r L - \sin \beta_r L}{\cosh \beta_r L + \cos \beta_r L}. \tag{10}$$

The eigenvalues of the cantilever beam with a fixed left-end can be calculated by

$$\cos \beta_r L \cosh \beta_r L + 1 = 0. \tag{11}$$

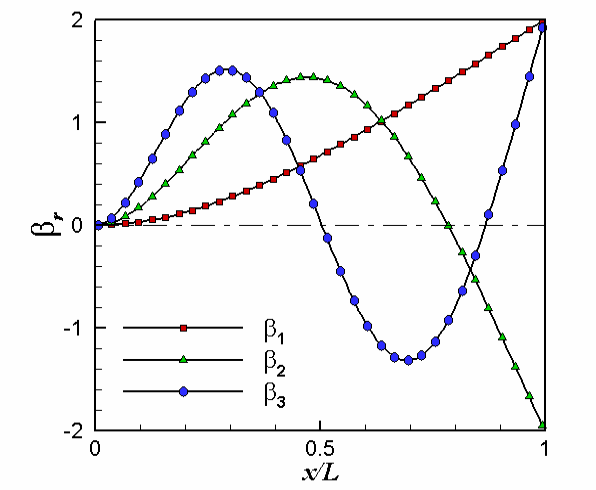

Figure 2 : Modal shapes of the cantilever beam

For approximations, only 3 eigenvalues are used: $\beta_1 L$=1.87510, $\beta_2 L$=4.69409, and $\beta_3 L$= 7.85476. The corresponding modal shapes obtained from Eq. (9) are presented in Fig. 2.

3 RESULTS AND DISCUSSION

3.1 Wake instability

The trailing-edge noise generated by wake instability is considered at Reynolds number based on a beam thickness, Re_h=200, free stream Mach number, M=0.4. As depicted in Fig. 3, the computational domain is extended from -400h to 300h in the streamwise direction and ±160h in the normal direction and non-uniform cartesian meshes of 301×211 points are distributed. A no-slip wall boundary condition is used at the solid surface, except the region from -400h to -200h, where a slip condition is applied. In order to induce the wake instability, a laminar boundary layer is disturbed with a vortical disturbance at tc_∞/L=40, which is defined as

$$u'(x,y) = \frac{1}{2h} U_0 (y - y_0) \exp\left(0.5 \left(1 - \left(\sqrt{(x-x_0)^2 + (y-y_0)^2} \,/\, h \right)^2 \right) \right)$$
$$v'(x,y) = -\frac{1}{2h} U_0 (x - x_0) \exp\left(0.5 \left(1 - \left(\sqrt{(x-x_0)^2 + (y-y_0)^2} \,/\, h \right)^2 \right) \right) \quad (12)$$

where the disturbance center is located at (x_o, y_o)=(0, 0.1L).

Figure 4 shows the vorticity and acoustic fields over the `rigid' cantilever at a periodic stage. The wake instability caused by Kelvin-Helmholtz instability produces a dipole tone from the trailing-edge. The pressure fluctuations monitored at (x/L, y/L)=(0, 2) indicates that the characteristic frequency is at $St_h = fh/U_0 \approx 0.046$ (or $\omega_c = 2\pi tL/c_\infty \approx 2.31$), which coincides

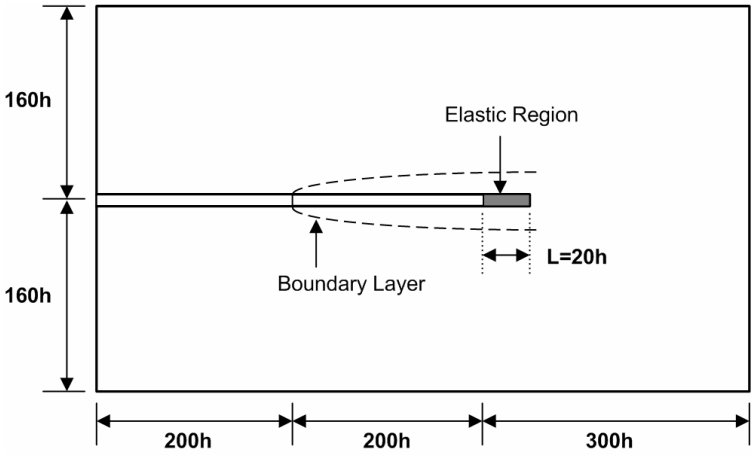

Figure 3 : Computational domain for the trailing-edge with an elastic cantilever end

with the most unstable mode[1] in the wake instability, and the predicted sound pressure level (SPL) at this frequency is about 109dB, as shown in Fig. 5.

In order to have the FSI effects, the rigid trailing-edge is replaced by an elastic cantilever beam. A non-dimensionalized natural frequency is defined as

$$\omega_r = (\beta_r L)^2 \frac{h}{c_\infty L}\sqrt{\frac{E}{12\rho}}, \tag{13}$$

where ρ and c_∞ indicate the material density and speed of sound, respectively. In the present study, a parametric study is conducted with various natural frequencies of the elastic cantilever beam by varying the elasticity E, while other parameters are kept constant, i.e.

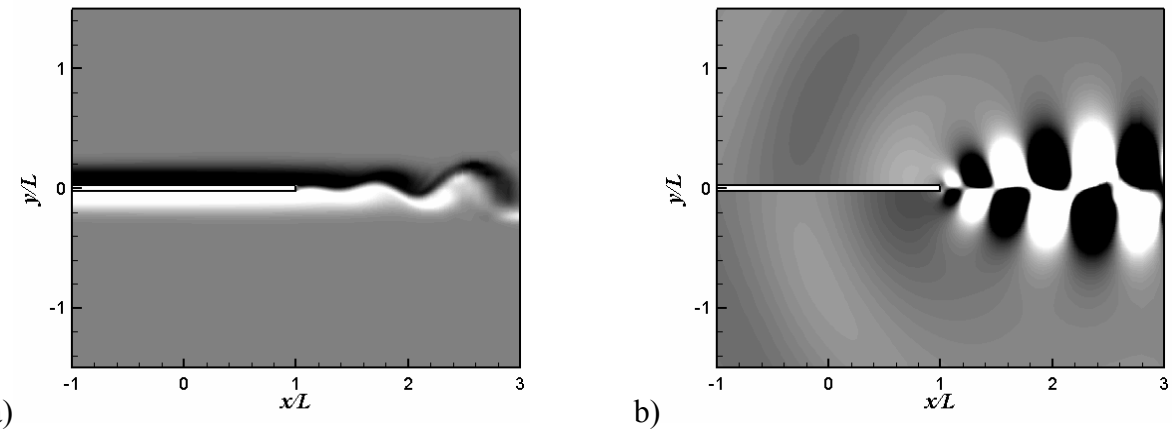

Figure 4 : Wake instability and the corresponding acoustic field around the rigid cantilever beam: a) vorticity (40 contours between -5 and 5), b) pressure fluctuation (40 contours between -0.002 and 0.002)

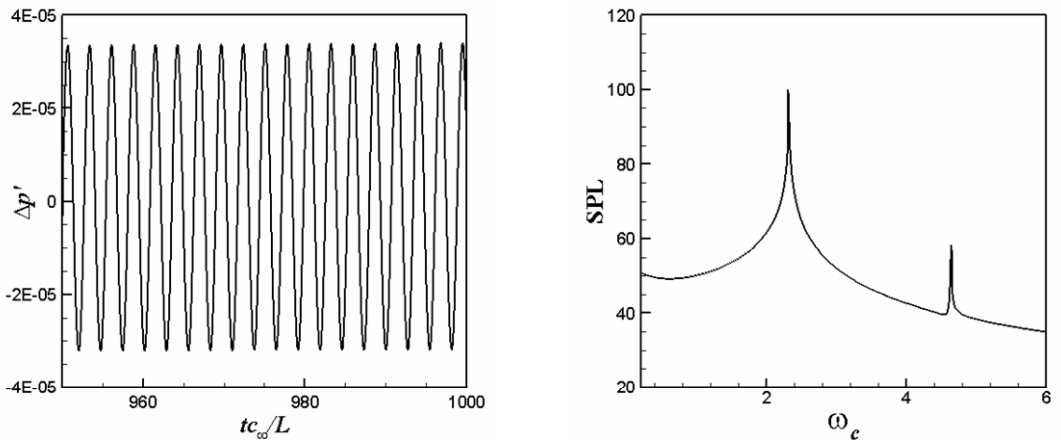

Figure 5 : Time variation of pressure fluctuations and SPL spectrum of the rigid trailing-edge at (x/L, y/L)=(0, 2): wake instability

ρ=240kg/m^3, c_∞=340m/s, and h/L=1/20. The objective is to find any FSI effect on the acoustic characteristics of the trailing-edge with elastic cantilever end. Test cases for the cantilever beams with various elastic properties are summarized in Table. 1.

Computed results indicate that tip displacement of the elastic trailing-edge is so small (maximum amplitude is about 0.0008h) that almost the same flow and acoustic characteristics are expected as compared to the rigid one. It is, however, found that the wake frequency is considerably modulated with this small tip displacement through FSI processes.

In Fig. 6, the modulated frequency ω_f and the SPL are plotted against a ratio between the first-eigenmode natural frequency of the elastic cantilever ω_n and the characteristic frequency of the wake ω_c. One can note a considerable variation not only in the modulated frequency but also in SPL for a range of -10% ~ +10% offsets from the resonant frequency, i.e. ω_n/ω_c=1. When ω_n/ω_c is 0.95, the wake characteristic frequency is altered from 2.31 to 2.22, whereas for ω_n/ω_c=1.05, it changes to 2.39. There are also two small variations at the second and third eigenmodes of the wake characteristic frequency, i.e. ω_n/ω_c=0.160 and ω_n/ω_c=0.057 but their effects are obviously much weaker than the first eigenmode.

Table 1 : Test cases for the cantilever beams with various elastic properties

	Density [kg/m^3]	Elasticitiy [Pa]	ω_1	ω_2	ω_3	ω_1/ω_c
Case A	240	1.91×10^8	0.132	0.825	2.310	0.057
Case B	240	6.39×10^8	0.241	1.510	4.226	0.104
Case C	240	1.50×10^8	0.369	2.310	6.468	0.160
Case D	240	6.72×10^8	0.781	4.896	13.709	0.338
Case E	240	5.87×10^8	2.310	14.477	40.535	1.000
Case F	240	1.36×10^8	3.516	22.034	61.697	1.522

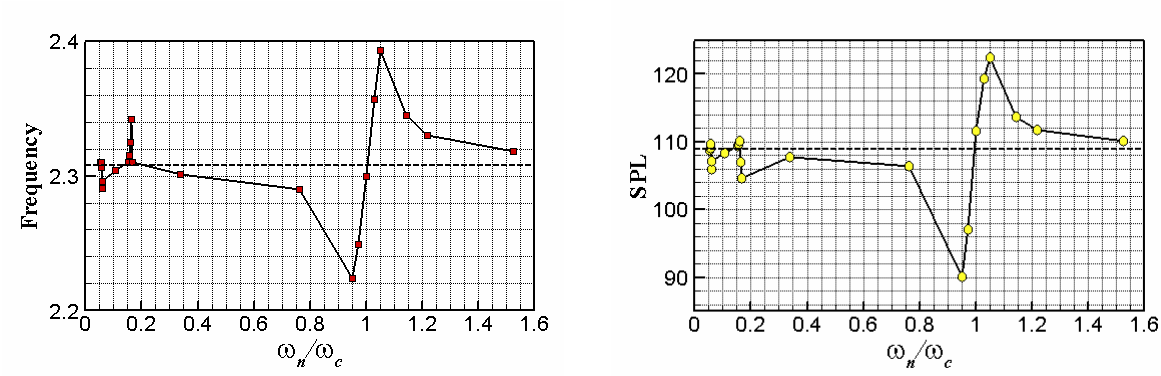

Figure 6 : Modulated frequency (ω_f) and sound pressure level (dB) at (x/L,y/L)=(0,2) versus natural frequency of the elastic cantilever (dashed line: rigid body)

A very similar variation of SPL against ω_n/ω_c is observed. When compared to the rigid body model, the trailing-edge noise with elastic cantilever end is significantly altered; decreased by 20dB at ω_n/ω_c=0.95 or increased by 15dB at ω_n/ω_c=1.05 (see Fig. 6). Figure 7 shows the directivities of the pressure fluctuations (at r=L) produced by the cantilever beams with various elastic properties. As expected, a major difference in directivity between the elastic and rigid trailing-edges occurs at ω_n/ω_c=0.95 and ω_n/ω_c=1.05. One can also note in the directivity pattern that noise reduction (ω_n/ω_c=0.95) occurs in all directions. It is also interesting to note that the SPL alteration is closely related to the frequency modulation, when eigen-natural frequencies of the cantilever are close to be resonant with the wake

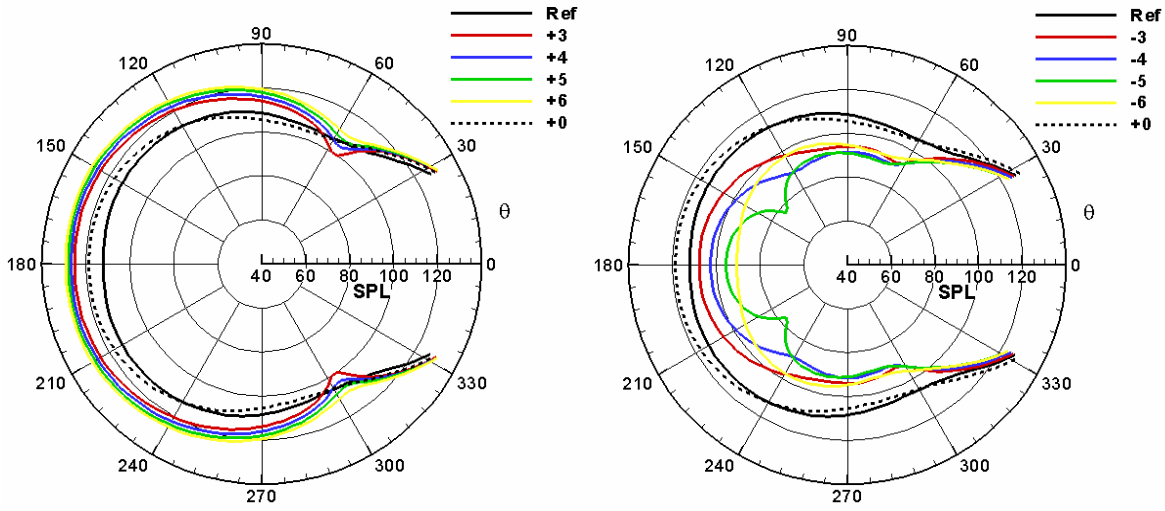

Figure 7: Directivity alterations with various elastic properties of the beam at r=L with a center (x/L, y/L)=(1, 0): wake instability

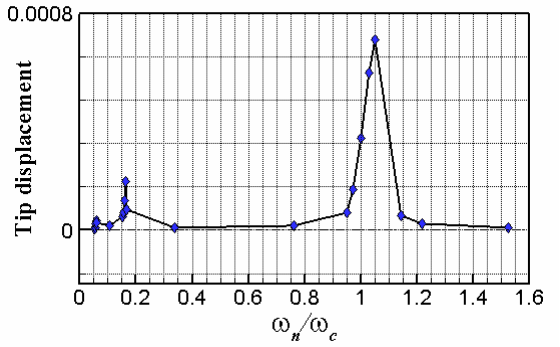

Figure 8 : Variation of tip displacement at various natural frequencies

characteristic frequency ω_c. In other words, the FSI process affects the wake frequency, SPL, and directivity pattern.

To clarify the relationship between the frequency modulation and the flow-induced vibration, the amplitude of the tip displacement is plotted in Fig. 8 against ω_n/ω_c. As expected, tip displacements are noticeably amplified at each eigen-resonant frequency (i.e. ω_{1n}/ω_c=1, ω_{2n}/ω_c=1, and ω_{3n}/ω_c=1). It is, however, interesting to note that the maximum tip displacement does not occur at ω_n/ω_c=1 but 1.05. This shift may be caused by a non-linear coupling between the unstable wake and the trailing-edge with elastic cantilever end. From these results, it is known that frequency modulation and SPL alteration are closely related to the tip displacement, even though their intimate correlations are still to be investigated.

In order to understand the vibration characteristics of the elastic cantilever, a forced-vibration calculation is carried out and compared with the FSI results. For the computation of forced-vibration, an external force is defined as

$$f(t) = q(x)\cos(\omega_c t), \tag{14}$$

where ω_c=2.31 and a distributed force $q(x)$ on the beam is modeled as

$$q(x) = \begin{cases} 0 & 0 \le x \le 0.5 \\ 0.0024\left(x-0.5\right)^2 & 0.5 \le x \le 1 \end{cases}. \tag{15}$$

As shown in Fig. 9(a), the tip displacement in forced-vibration continuously increases at the resonant frequency (0% offset), while beats are clearly observed for ±5% offset cases. But the FSI cases show different dynamical behaviors in Fig. 9(b). At resonance frequency, tip displacement increases initially but converges to an asymptotic value because fluids act as a damper to the cantilever beam motions. When a natural frequency is ±5% offset from the wake characteristic frequency, beats gradually disappear and the wake frequency is modulated into a value close to the natural frequency of the elastic cantilever. The most amplified tip displacement occurs at +5% offset. Thus, it is known that frequency modulation near the resonance frequency alters the dynamic characteristics of the trailing-edge and eventually

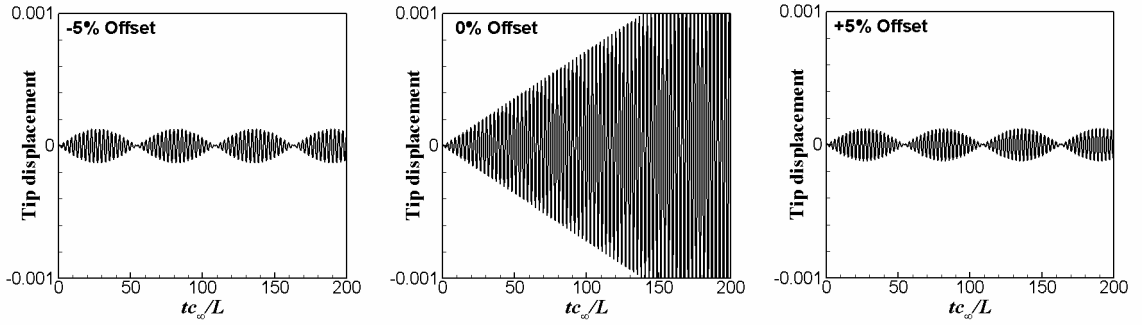

(a) Forced-vibration

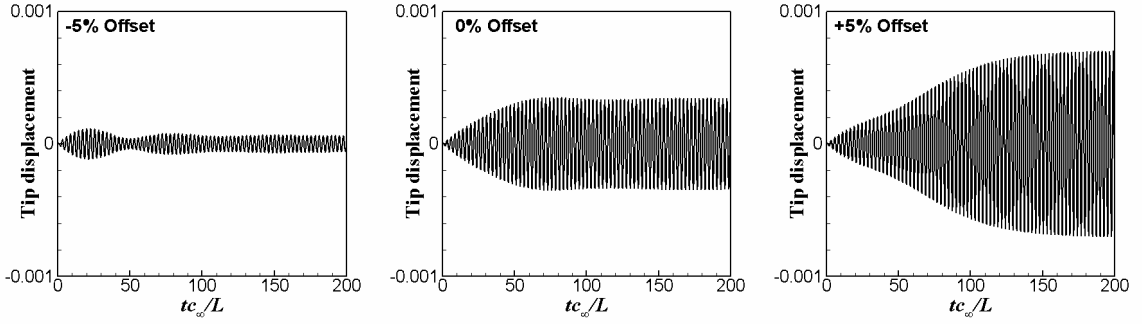

(b) Fluid-structure interaction

Figure 9 : Time variation of tip displacement

influences the flow and sound fields.

3.2 Karman vortex shedding

For further investigation of FSI effects on the trailing-edge noise, similar computations are conducted for the case of Karman vortex shedding. A laminar boundary layer is considered over the trailing-edge at Reynolds number based on the beam thickness, Re_h=1000, free stream Mach number, M=0.4. The computational domain and grid system are the same as the wake instability. A no-slip wall boundary condition is applied from -1.5L so that the boundary layer thickness at the trailing-edge is 1.2h. This value is an upper limit (laminar) to invoke the Karman vortex shedding[1] with a blunt thickness.

Figure 10 shows the flow and acoustic fields for the rigid cantilever beam at a periodic stage. Due to the bluntness of the trailing-edge, the Karman vortex shedding produces a dipole tone at the edge. Computed results at the monitoring position indicate that the characteristic frequency of the vortex shedding is at $St_h=fh/U_0\approx0.145$ (or ω_c=7.28), and the SPL is about 135dB at this frequency (see Fig. 11). According to Fig. 12, frequency modulation also occurs near $\omega_n/\omega_c=1$, similar to the wake instability case (see Fig. 6). The directivity alteration with various elastic properties of the beam is shown in Fig. 13. A major difference in SPL between the elastic and rigid trailing-edges occurs, when the first-eigenmode natural frequency of the cantilever is

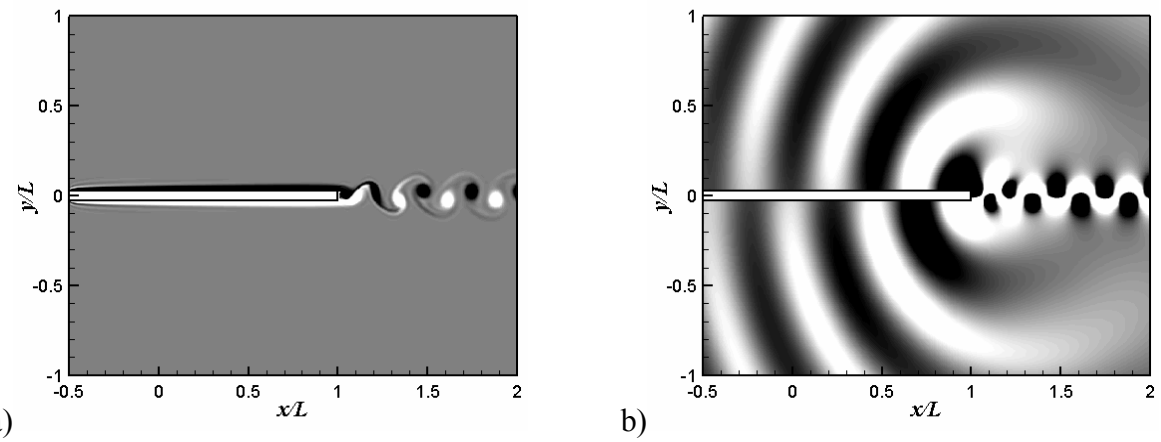

Figure 10 : Karman vortex shedding and the corresponding acoustic field around the rigid cantilever beam: a) vorticity (40 contours between -5 and 5), b) pressure fluctuation (40 contours between -0.002 and 0.002)

±2% offset from ω_c.

The FSI effects on acoustic characteristics are somewhat different from the wake instability. Noise reduction occurs partially with angles from -120^o to +120^o. Also, noise is even reduced for the positive offsets from ω_c but not as much as the negative cases. The FSI effects are not so substantial as the wake instability because vortex shedding is a very localized phenomenon at the trailing-edge. If density of the material changes, more pronounced alterations in SPL are expected. Further investigations will be reported in one of the upcoming presentations.

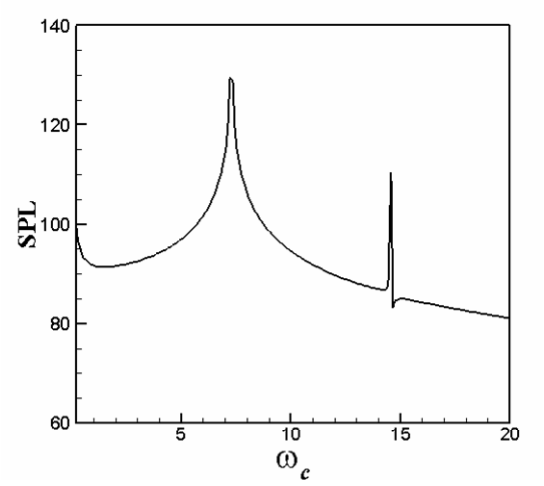

Figure 11 : SPL spectrum for the rigid trailing-edge at (x/L, y/L)=(0, 2): Karman vortex shedding

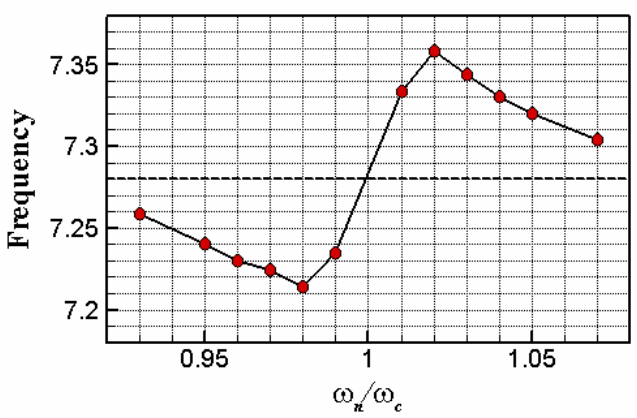

Figure 12 : Modulated frequency (ω_f) versus natural frequency of the elastic cantilever (dashed line: rigid body)

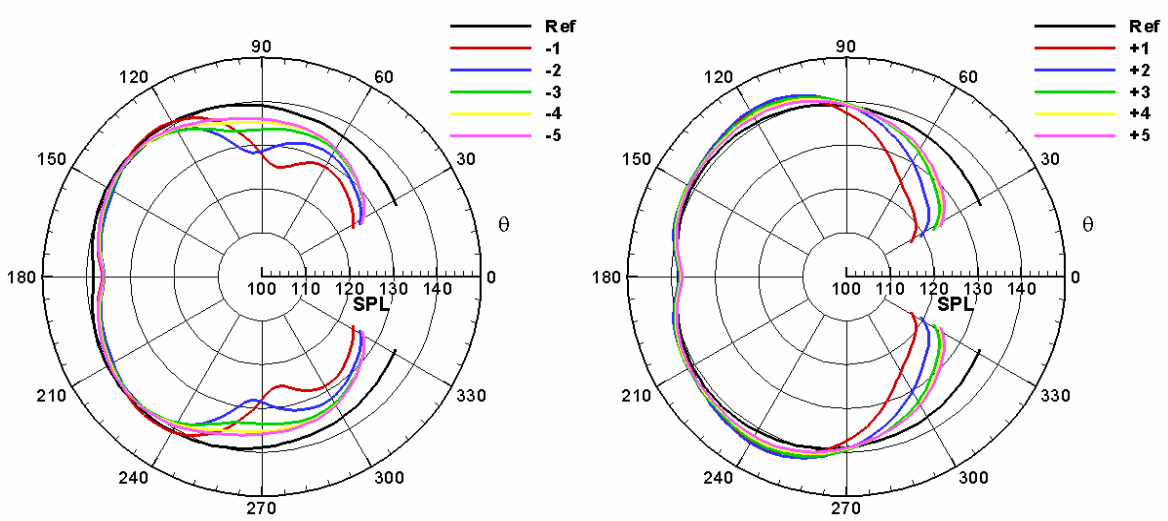

Figure 13 : Directivity alterations with various elastic properties of the cantilever at r=L with a center (x/L, y/L)=(1, 0): Karman vortex shedding

4 CONCLUSIONS

In this study, the FSI effects on the trailing-edge noise have been investigated for the wake instability (Re_h=200 and Ma=0.4) and Karman vortex shedding (Re_h=1000 and Ma=0.4). The FSI effects are scrutinized with various elastic properties of the cantilever beam. From the computed results, it can be concluded that

- when the first-eigenmode natural frequency of the cantilever is near the characteristic frequency of the flow (within the range of -10% ~ +10%), the frequency modulation results in noise reduction of 20dB in all directions (wake instability), or 10-12dB partially (Karman vortex shedding)

- the tip displacement of the elastic trailing-edge is closely related to the frequency modulation as well as the SPL
- beats observed in force-vibration do not occur in FSI process by fluid-damping.

REFERENCES

[1] W.K. Blake, *Mechanics of Flow-Induced Sound and Vibration, Vol. 1, General concepts and elementary sources*, Academic Press (1986).
[2] T.F. Brooks and T.H. Hodgson, "The trailing-Edge Noise Prediction From Measured Surface Pressure", *Journal of Sound and Vibration*, Vol. 78, No. 1, 69-117 (1981).
[3] M.S. Howe, "A Review of the Theory of Trailing-Edge Noise", *Journal of Sound and Vibration*, Vol. 61, No. 3, 437-465 (1978).
[4] M. Roger and S. Moreau, "Broadband Self-Noise from Loaded Fan Blades", *AIAA Journal*, Vol. 42, No. 3, 536-544 (2004).
[5] M. Wang and P. Moin, "Wall Modeling in LES of Trailing Edge Flow", *Proc. 2nd Int. Sympo. On Turbulence and Shear Flow Phenomena*, Stockholm, Sweden, II, 165-170 (2001).
[6] K.W. Chang, J. H. Seo, Y.J. Moon, and M. Roger, "Prediction of Flat Plate Self-Noise", *AIAA-Paper* 2006-2513 (2006).
[7] J.H. Seo and Y.J. Moon, "The Linearized Perturbed Compressible Equations for Aeroacoustic Noise Prediction at Very Low Mach Numbers", *AIAA-Paper* 2005-2927 (2005).
[8] A.L. Marsden and M. Wang, and B. Mohammadi, "Shape Optimization for Aerodynamic Noise Control", *Center for Turbulence Research, Annual Research Briefs* (2001).
[9] M.R. Khorrami and M.M. Choudhari, "Application of Passive Porous Treatment to Slat Trailing Edge Noise", *Langley Research Center, NASA/TM* 2003-212416 (2003).
[10] M. Herr and W. Dobrzynski, "Experimental Investigation in Low Noise Trailing Edge Design", *AIAA-Paper* 2004-2804 (2004).
[11] S.K. Lele, "Compact Finite Difference Schemes with Spectral-Like Resolution", *Journal of Computational Physics*, Vol. 103, 16-42 (1992).
[12] D. Gaitonde, J.S. Shang, and J.L. Young, "Practical Aspects of High-Order Accurate Finite-Volume Schemes for Electrmagnetics", *AIAA-Paper*, 97-0363 (1997).
[13] N.B. Edgar and M.R. Visbal, "A General Buffer Zone-Type Non-Reflecting Boundary Condition for Computational Aeroacoustics", *AIAA-Paper*, 2003-3300 (2003).
[14] L. Meirovitch, *Fundamentals of Vibrations*, McGraw-Hill (2001).
[15] M.P. Paidoussis, Fluid-*Structure Interactions Volume I*, Academic Press (1998).